Theoretical Studies for the Structural Properties and Electron Transfer Reactivity of $C_4H_5N/C_4H_5N^+$ Coupling System

Qiao Sun,[†,‡] Yuxiang Bu,*[,†,‡] and Mei Qin[‡]

Institute of Theoretical Chemistry, Shandong University, Jinan, 250100, P. R. China, and Department of Chemistry, Qufu Normal University, Qufu, 273165, P. R. China

Received: July 27, 2002; In Final Form: January 3, 2003

The geometries and vibrational frequencies of pyrrole, pyrrole cation, and their corresponding encounter complexes have been determined using density functional theory (DFT) and/or ab initio methods with 6-31G* and/or 6-311+G* basis sets. Optimizations indicate that there are three stable complex modes. One mode has the ring−ring parallel contact (face−face) and each N atom in two rings is vertically over the center of another ring (complex 1). In the second mode (complex 2), two rings are also parallel, but they are directly contacted by only one N−C bond in each ring (side-side). The third mode (complex 3) is H−bond mode, in which the N−H of one pyrrole ring is nearly collinearly directed to the N center of another pyrrole ring and two rings are perpendicular to each other. For three-encounter complexes, their main bond lengths are between those of the pyrrole and those of the pyrrole cation. The character contact distances are 2.754 Å (C3···C13), 2.727 Å (C3···C12), and 2.632 Å (N1···H16) at the B3P86/6-31G* level, respectively. The stabilization energies of the three encounter complexes are calculated to be 21.4 (complex 1), 20.2 (complex 2), and 15.9 (complex 3) kcal/mol at the B3LYP-DFT/6-311+G* level with the correction for BSSE. The inapplicability of DFT methods has been discussed in predicting the energy curves, especially with long contact distance in which the DFT methods give the abnormal behavior for the dissociation of the complexes due to the "inverse symmetry breaking" problem. On the basis of three stable encounter complexes, three coupling modes have been designed by keeping the relative orientation and changing the contact distance for further investigating electron-transfer reactivity. The contact distance dependences of the activation energy, the coupling matrix element, and the electron-transfer rate have also been determined at the MP2/6-31G* level. Electron transfer can occur over a range of encounter distance. For the $C_4H_5N/C_4H_5N^+$ coupling system, electron transfer occurs chiefly over a range of contact distances where $2.0 < R_{a-b} < 6.0$ Å. The most favorable coupling mode to electron transfer is the coupling mode 3, which is related to complex 3. It should be noted that it is not always true that the electron transfer must take place via the most stable encounter complex mechanism. For the $C_4H_5N/C_4H_5N^+$ systems, the most stable encounter complex is complex 1, but the most favorable coupling mode for the electron transfer is coupling mode 3, depending on the different contact distance ranges.

1. Introduction

Pyrrole, its cation, and its ramifications exist widely as constituents of biological macromolecules. For example, pyrrole is a building block of several important biological molecules such as amino acids, nucleotide bases, and more. Pyrrole and its cation have been investigated extensively with both experimental[1,2] and theoretical[3−5] methods, but the studies of the different coupling modes between pyrrole and its cation have not been reported elsewhere. In the biological systems, pyrrole ring is linked to the amino acid residues and other biological molecular chains, the interaction of the pyrrole ring with the other groups and biologically active ions such as H-bond interaction, dipole−dipole interaction, electrostatic interaction, and other weak interactions play a very important role in assisting the biological functionality. Obviously, the intermediate molecular fragments linked to the donor−acceptor active sites play the dominant role in assisting and promoting the ET and the proton translocation and further affecting the biological functionality. Therefore, it is fundamental to explore the coupling interaction modes, H-bond mechanism, and the ET reactivity of this kind of heteroring systems for the further understanding of the biological functional mechanism. In this article our emphasis will be on the complexes formed between pyrrole and its cation, and their ET reactivity.

In the past two decades, ET reactions have continued to be the subject of many theoretical[6−10] and experimental[11−14] studies, no matter for the chemistry systems or the biological systems. In general, the ET can occur in a determinate range of contact distance, although there is a maximum reaction probability for each ET system in an optimum contact distance. However, for a real system, especially for a biological system, since the active donor−acceptor groups are generally fixed to the biological molecular chains, the structural constraint and the solvent fluctuation perhaps cannot assuredly give the donor−acceptor species an optimum interaction mode for favoring the ET like that for gas phase isolated coupling couple. Therefore it is very interesting to investigate the ET reactivity of the system at the different contact distances and the coupling mode effect on the ET mechanism. However, although there are many publications

* Corresponding author.
† Shandong University.
‡ Qufu Normal University.

10.1021/jp026622j CCC: $25.00
Published on Web 02/12/2003

which aim at the ET reactivity of the various systems, studies on the coupling mode (including contact distance and orientation, etc.) dependence of the ET reactivity for any systems are seriously lacking. In detail for the pyrrole ion pair, studies on the interaction mode and the ET mechanism have also not been reported elsewhere up to now. Therefore in this paper, taking the pyrrole/pyrrole cation pair as model species, accurate descriptions of kinetics parameters of the self-exchange ET reaction of pyrrole and pyrrole cation will be made, and the contact distance dependence of various kinetics parameters such as the activation energy, the coupling matrix element, and the electron-transfer rate of the $C_4H_5N/C_4H_5N^+$ coupling system will be analyzed.

In addition, in view of the complication of the biological macromolecule and the computational cost at wave function correlated ab initio theoretical levels, computational methods based on density functional theory (DFT) have been widely used. These methods can predict relatively accurate molecular structures and vibrations with moderate computational effort for the equilibrium systems. However, for the ET systems mentioned above, the ET or the proton transfer occurring must not require the donor and acceptor to be the most favorable geometries and interaction modes. Once the ET or proton transfer condition is met, the transfer may occur with a considerable probability regardless of the coupling system in the equilibrium geometry or in the nonequilibrium geometry. So in order to explore the electron transfer reactivity of the system at a geometry far from the equilibrium geometry, it is very important to determine its global potential energy surface. Therefore, this work also presents a challenge for the theoretical calculational methods to determine which may be suitable for the calculations on the systems at the geometry far from equilibrium.

A recent study has indicated that the energy curves with some DFT methods (such as B3LYP, B3P86, etc.) present an abnormal dissociation behavior. This abnormal behavior was first reported by Bally and Sastry in 1997[15] and was recognized to be due to the "inverse symmetry breaking" problem. In view of this consideration, another goal of this paper is to check the applicability of DFT methods and the wave function correlated ab initio methods in predicting the energy curves, especially in range of long contact distances, and to test any abnormal behavior. So both DFT and the second-order Møller−Plesset theory methods are used in this paper.

2. Theoretical Scheme

The self-exchange ET reaction between the neutral pyrrole and its cation can be expressed as eq 1

$$C_4H_5N(R_1) + C_4H_5N^+(R_2) = C_4H_5N^+(R_2) + C_4H_5N(R_1) \quad (1)$$

where R_1 and R_2 denote the characteristic geometric parameters such as bond lengths, bond angles, and dihedral angles of the neutral pyrrole and its cation, respectively, and may be expressed as $R_1 = \{q_1^1, q_1^2, q_1^3, ...\}$ and $R_2 = \{q_2^1, q_2^2, q_2^3, ...\}$, where q_i^j is refers to bond length, bond angle, etc. They are functions of the reaction coordinate in the reaction process.

There are five elementary processes of the ET between the donor (C_4H_5N) and the acceptor ($C_4H_5N^+$):

(1) formation of the encounter complex

$$C_4H_5N(R_1) + C_4H_5N^+(R_2) \rightarrow C_4H_5N(R_1')\cdots C_4H_5N^+(R_2') \quad (2)$$

(2) reorganization of the encounter complex

$$C_4H_5N(R_1')\cdots C_4H_5N^+(R_2') \rightarrow C_4H_5N(R_1^*)\cdots C_4H_5N^+(R_2^*) \quad (3)$$

(3) electron transfer

$$C_4H_5N(R_1^*)\cdots C_4H_5N^+(R_2^*) \rightarrow C_4H_5N^+(R_1^*)\cdots C_4H_5N(R_2^*) \quad (4)$$

(4) relaxation of successor activated complex

$$C_4H_5N^+(R_1^*)\cdots C_4H_5N(R_2^*) \rightarrow C_4H_5N\,(R_1'')\cdots C_4H_5N^+\,(R_2'') \quad (5)$$

(5) dissociation of successor complex

$$C_4H_5N\,(R_1'')\cdots C_4H_5N^+(R_2'') \rightarrow C_4H_5N^+(R_2) + C_4H_5N(R_1) \quad (6)$$

where R_1' and R_2' are the corresponding R_1 and R_2 in the encounter complex, and R_1'' and R_2'' are those in the successor complex. R_1^* and R_2^* are the activated geometrical parameters corresponding to R_1 and R_2 in the activated state.

Obviously, the product of eq 2 is the encounter complex and may have various different structures. Equation 2 is the preequilibrium equation; the energy change corresponds to the sum of the electrostatic work required to bring the reactants together and the stabilization energy. The energy change in eq 3 corresponds to the activation energy.

There are many quantum-mechanical theories that have been successfully used to discuss the relationship between the ET rate and some parameters.[16,17] Among these theories, Golden-rule is an excellent one. Golden-rule has been successfully used to deal with ET of $O_2+O_2^-$ and hydrogen transfer tunneling reaction.[18,19] In this paper, Golden-rule is used to discuss the contact distance dependence of kinetics parameters such as the activation energies, the coupling matrix elements, and the electron transfer rates of the $C_4H_5N/C_4H_5N^+$ system. According to Golden-rule, the rate of ET can be expressed as the following equation

$$k_{et}(R_{a-b}) = (4\pi^2/h)|H_{if}(R_{a-b})|^2\,FC(R_{a-b}) \quad (7)$$

where H_{if} is the coupling matrix element between the two redox active sites, FC is the Franck−Condon factor, and h is Planck's constant. R_{a-b} is the definite contact distance.

A simple formula of the coupling matrix element can be expressed as the following eq 8, and it has been successfully used to calculate ET kinetics parameters of many systems.[17,20] H_{if} may be directly expressed as a simple formula described in eq 8

$$H_{if}(R_{a-b}) = E_d - E_a(R_{a-b}) \quad (8)$$

where H_{if} actually represents the energy difference between the nonadiabatic activated state and the adiabatic activated state. $E_a(R_{a-b})$ denotes the adiabatic activation energy and E_d denotes the nonadiabatic activation energy, which is the energy of reacting system at the crossing point under the assumption that the reacting system experiences a nonadiabatic electron transmission process.

FC originates from the requirement (Franck−Condon principle) that the nuclear configuration of the reactants must be kept unchanged when the electron transfers. There are two factors influencing FC factor, which are the free energy and the reorganization energy. The FC factor may be directly expressed as a simple formation

$$\mathrm{FC}(R_{a-b}) = (4\pi E_\lambda(R_{a-b})RT)^{-1/2} \exp(-E_a(R_{a-b})/RT) \quad (9)$$

where $E_\lambda(R_{a-b})$ and $E_a(R_{a-b})$ denote the reorganization energy and the activation energy at different contact distances, respectively, and T is the thermodynamic temperature. For a thermoneutral exchange process, $E_\lambda = 4E_a$ under the harmonic approximation.

At the activated state, the energy of the activated complex $C_4H_5N(R_1^*)\cdots C_4H_5N^+(R_2^*)$ before ET can be expressed as the following formation:

$$E_i = E_{C4H5N}(R_1^*) + E_{C4H5N}{}^+(R_2^*) \quad (10)$$

After the ET, the energy of the product complex may be expressed as

$$E_f = E_{C4H5N}{}^+(R_1^*) + E_{C4H5N}(R_2^*) \quad (11)$$

where $E_j(R^*)$ denotes the energy of jth molecular fragment species in the reacting complex at the activated state [$C_4H_5N\cdots C_4H_5N^+$]. During the transition, the energy conservation principle requires that $E_f = E_i$. Thus

$$E_{C4H5N}(R_1^*) + E_{C4H5N}{}^+(R_2^*) = E_{C4H5N}{}^+(R_1^*) + E_{C4H5N}(R_2^*) \quad (12)$$

Since C_4H_5N and $C_4H_5N^+$ are two systems with different properties, eq 12 suggests that R_1^* should be equal to R_2^*. Therefore, the energy of the system at the activated state can be expressed as

$$E_a^* = E_{C4H5N}(R_1^*) + E_{C4H5N}{}^+(R_2^*) \quad (13)$$

Obviously eq 13 represents the energy curve formed in the crossing between the two nonadiabatic potential energy surfaces corresponding to the initial and the final states of the ET, respectively.

The adiabatic activation energy $E_a(R_{a-b})$ can be easily obtained by subtracting the energy of the encounter complex from the corresponding energy at the activated state, viz.

$$E_a(R_{a-b}) = E_{C4H5N^+\cdots C4H5N}(R_1^*,R_2^*,R_{a-b}) - E_{C4H5N^+\cdots C4H5N}(R_1',R_2', R_{a-b}) \quad (14)$$

Actually this state intuitively represents the geometry that the ET is likely to take place.

Analogously, the nonadiabatic activation energy can be obtained by subtracting the energies of C_4H_5N and $C_4H_5N^+$ at their own equilibrium geometries from the total energies of C_4H_5N and $C_4H_5N^+$ at the crossing point.

$$E_d = E_{C4H5N}(R_1^*) + E_{C4H5N}{}^+(R_2^*) - E_{C4H5N}(R_1) - E_{C4H5N}{}^+(R_2) \quad (15)$$

Thus, the electronic coupling matrix element or the energy reduction caused by the coupling between the initial and the final states of ET may be obtained by

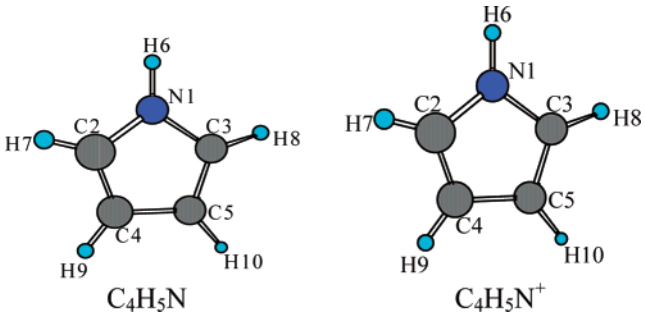

Figure 1. Atomic numbering corresponding to the geometrical parameters of neutral pyrrole and pyrrole cation.

$$H_{if}(R_{a-b}) = E_d - E_a(R_{a-b})$$

$$H_{if}(R_{a-b}) = E_{C4H5N}(R_1^*) + E_{C4H5N}{}^+(R_2^*) - E_{C4H5N}{}^+\cdots{}_{C4H5N}(R_1^*,R_2^*,R_{a-b}) - E_s(R_{a-b}) \quad (16)$$

$$E_s(R_{a-b}) = E_{C4H5N}(R_1) + E_{C4H5N}{}^+(R_2) - E_{C4H5N}{}^+\cdots C4H5N(R_1',R_2', R_{a-b}) \quad (17)$$

3. Calculation Details

All calculations are performed with the GAUSSIAN94 program[21] using three density functional methods (B3LYP, B3P86, and B3PW91) and MP2 method with 6-31G* and/or 6-311+G* basis sets. These three B3LYP, B3P86, and B3PW91 DFT models combine Becke three-parameter hybrid functional, which is a linear combination of Hartree−Fock exchange, the correlation functional of Lee, Yang, and Parr,[22,23] Perdew (P86),[24,25] Perdew and Wang (PW91),[26] respectively.

The geometries and vibrational frequencies of pyrrole, pyrrole cation, and three encounter complexes are first optimized using DFT and/or ab initio methods with 6-31G* and/or 6-311+G* basis sets. The geometries have been displayed in Figures 1 and 2. Then, the Mulliken population analyses are made, and the total net charges and the bond overlap populations are obtained for C_4H_5N, $C_4H_5N^+$, complex 1, complex 2, and complex 3 at the B3P86/6-31G* level. Second, the stabilization energies (kcal/mol) of the three complexes are calculated with three DFT methods (B3LYP, B3P86, and B3PW91) using 6-31G* and 6-311+G* basis sets. The correction for basis set superposition error[21] (BSSE) has been performed for obtaining more accurate results using the 6-31G* basis set. To further investigate the effect of the coupling mode and contact distance on the ET reactivity, on the basis of the obtained three stable encounter complexes, three coupling modes are designed (cf. Figure 2). In detail, these three coupling modes actually correspond to the three stable encounter complexes. For the coupling mode 1, the relative orientation of two pyrrole rings is kept unchanged, compared with the stable encounter complex 1, and the C3···C13, the direct contact distance between two rings, is selected as the contact distance (R_{a-b}, the reaction coordinate, or the scanning variable). Namely, two pyrrole rings may shift according to the arrow direction displayed in Figure 2. Actually, this mode is referred to as the face−face coupling mode. Similarly, for the coupling mode 2, the relative orientation is the same as the encounter complex 2; the distance between C3 and C12 is defined as the contact distance (R_{a-b}). The corresponding arrow direction is the relative shift direction of the two rings. For the coupling mode 3, it originates from the

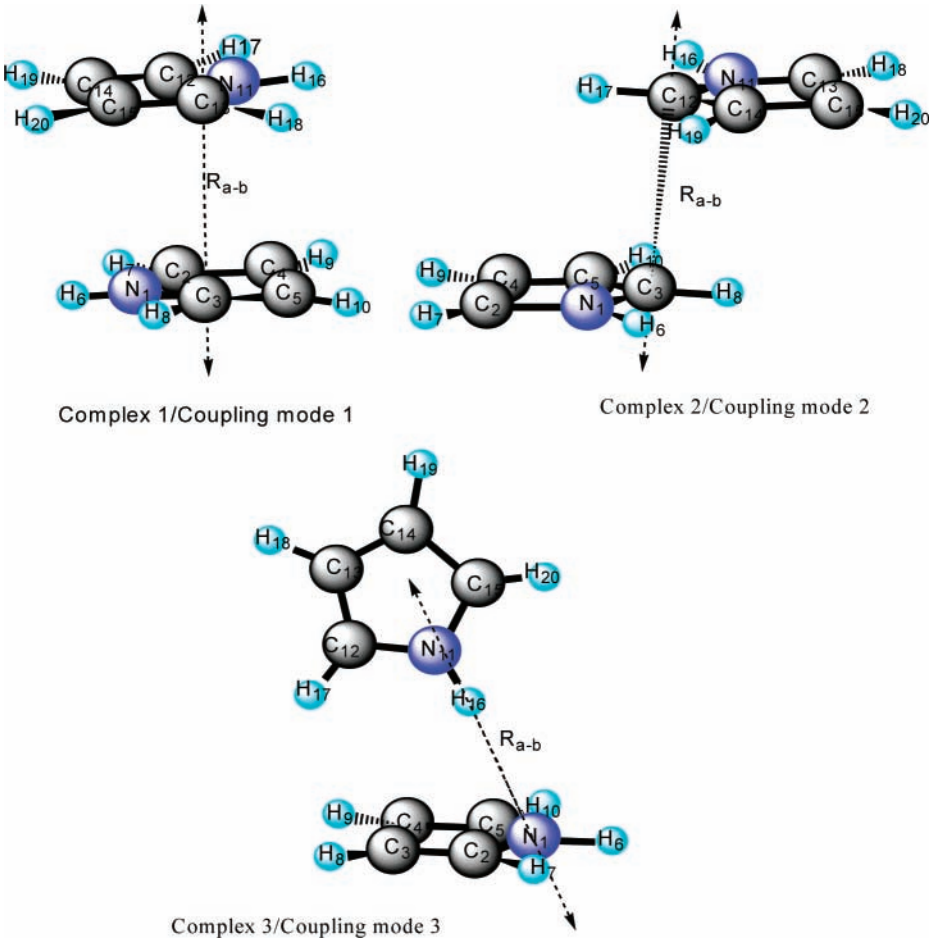

Figure 2. Structures and relative ring orientations of three coupling modes between neutral pyrrole and its cation. At the optimized geometries, they correspond to three different stable encounter complexes.

interaction between the N−H of the one pyrrole ring and the N site of the other pyrrole ring by forming a H bond along the N···H···N line. Keeping the relative orientation of the complex 3, taking the N1−H16 bond length as the contact distance (R_{a-b}), the two rings may move relatively, according to the arrow direction in complex 3. According to the above-defined three coupling modes, the potential energy surfaces have been determined with respect to the contact distances. Therefore, the applicability of DFT methods (B3LYP, B3P86) and the MP2 method in exploring the potential energy surface at the activated state has also been checked. In view of the reasonableness of the MP2 curves, the MP2 method with the 6-31G* basis set is used to scan the potential energy surfaces in order to obtain the relevant energy quantities (such as activation energy, etc.), the coupling matrix elements, and Franck−Condon factors of this system. Finally, the contact distance dependence of the kinetics parameters is discussed. In addition, it should be noted that in the scan optimizations, all bond lengths and the other bond angles are optimized, while the relative orientation between two pyrrole fragments is constrained.

4. Results and Discussion

4.1. Geometric Structures and Vibrational Frequencies of Pyrrole and Its Cation. In this section we present and discuss the results of the geometric structures and vibrational frequencies of pyrrole then compare them with other ab initio results and the available experimental data in order to choose suitable methods and basis set for pyrrole cation and the three-encounter complexes (dimeric cation) formed from pyrrole and its cation.

Pyrrole has been investigated extensively with both experimental[1,2] and theoretical[3−5] methods, so these studies have presented many opportunities to compare our calculated data with corresponding experimental data and the previously calculated data. The bond lengths (Å), the bond angle (deg), the rotational constant (GHz), and the dipole moment of pyrrole calculated by using the MP2(full), B3P86, B3LYP, and B3PW91 methods with 6-31G*and 6-311+G* basis sets are displayed in Table 1. Analysis has indicated that the results obtained with several methods and basis sets are close to each other, they are also in good agreement with the experimental values and the other theoretical values.[1,3,4] In addition, the dipole moment results given in Table 1 for pyrrole also appear to be very close to each other for several methods; they are slightly larger by 0.2 D than the experimental data. This good agreement implies the applicability of these methods in the further calculations concerning the pyrrole cation and the encounter complexes. Therefore, the MP2(full) with full electron correlation including the inner-shell electrons and DFT(B3P86, B3LYP and B3PW91) methods with 6-31G* and 6-311+G* basis sets are chosen to investigate the geometrical structure of pyrrole cation. As to the three complexes, in view of such a fact that the ab initio MP2(full) method takes more disk space and CPU time than DFT methods with the same basis set, only DFT levels (B3P86, B3PW91, and B3LYP) using the 6-31G* basis set are chosen

TABLE 1: Computed Equilibrium Bond Lengths (Å), Bond Angles (deg), Rotational Constants (GHz), Zero-Point Vibrational Energies (kcal/mol), and Dipole Moments (Debye) of Pyrrole

	B3P86 6-31G*	B3LYP 6-31G*	B3PW91 6-31G*	B3P86 6-311+G*	B3LYP 6-311+G*	B3PW91 6-311+G*	MP2(FULL) 6-311+G*	expt[a]
				Bond Lengths				
N1−H6	1.007	1.008	1.007	1.005	1.006	1.005	1.008	0.996
N1−C2	1.370	1.375	1.371	1.369	1.375	1.370	1.372	1.370
C2−C4	1.376	1.378	1.377	1.374	1.377	1.376	1.387	1.382
C4−C5	1.421	1.425	1.422	1.420	1.425	1.421	1.421	1.417
				Bond Angles				
H6−N1−C2	125.0	125.1	125.0	125.1	125.1	125.1	124.9	125.1
C2−N1−C3	109.9	109.8	109.9	109.9	109.8	109.9	110.2	109.8
N1−C2−C4	107.7	107.7	107.7	107.7	107.7	107.7	107.5	107.7
C2−C4−C5	107.4	107.4	107.4	107.4	107.4	107.4	107.4	107.4
N1−C2−H7	121.2	121.1	121.1	121.2	121.2	121.2	121.3	121.3
C2−C4−H9	125.7	125.7	125.8	125.7	125.7	125.7	125.5	125.7
				Rotational Constants				
A	9.191	9.134	9.174	9.204	9.144	9.188	9.146	8.951
B	9.044	9.002	9.027	9.063	9.017	9.047	8.965	8.890
C	4.558	4.534	4.550	4.567	4.540	4.559	4.527	4.460
				Zero-Point Vibrational Energies				
	52.15	51.85	52.08	51.81	51.52	51.74	51.25	51.78
				Dipole Moments				
				1.943	1.915	1.947	1.965	1.74

[a] References 1 and 5.

TABLE 2: Computed Equilibrium Bond Lengths (Å), Bond Angles (deg), Rotational Constants (GHz), and Zero-Point Vibrational Energies (kcal/mol) of Pyrrole Cation

	B3P86 6-31G*	B3LYP 6-31G*	B3PW91 6-31G*	B3P86 6-311+G*	B3LYP 6-311+G*	B3PW91 6-311+G*	MP2(FULL) 6-311+G*
				Bond Lengths			
N1−H6	1.014	1.015	1.015	1.012	1.013	1.012	1.014
N1−C2	1.359	1.363	1.360	1.357	1.362	1.358	1.359
C2−C4	1.430	1.434	1.432	1.428	1.432	1.430	1.433
C4−C5	1.371	1.374	1.372	1.368	1.372	1.369	1.377
				Bond Angles			
H6−N1−C2	125.5	125.5	125.5	125.5	125.5	125.5	125.4
C2−N1−C3	109.1	109.0	109.1	109.1	109.1	109.0	109.2
N1−C2−C4	108.3	108.3	108.4	108.3	108.3	108.3	108.4
C2−C4−C5	107.1	107.2	107.7	107.1	107.2	107.1	107.0
N1−C2−H7	121.7	121.7	121.7	121.6	121.7	121.6	121.6
C2−C4−H9	124.8	124.7	124.8	124.8	124.8	124.8	124.9
				Rotational Constants			
A	9.485	9.432	9.470	9.514	9.457	9.502	9.439
B	8.594	8.552	8.577	8.621	8.573	8.604	8.557
C	4.509	4.485	4.501	4.523	4.497	4.515	4.488
				Zero-Point Vibrational Energies			
	51.84	51.59	51.78	51.60	51.34	51.54	

to optimize the geometrical structures of the encounter complexes.

For the sake of convenient comparison, we choose the data calculated by the same method (B3P86) and the same basis set (6-31G*) to analyze the geometry structure of pyrrole, pyrrole cation, and three complexes, then to discuss the relation of the bond length with the overlap population.

Pyrrole has been shown to have C_{2v} symmetry in gas phase[3] and it is a compound of five-membered heterocyclic aromatic ring, in which a lone pair of electrons offered by the N atom and the two double bonds form a delocalized big π-bond. Table 4 lists the Mulliken population analysis results. Although this electronic population analysis scheme is, strictly speaking, unreasonable, it can also predict an approximate regularity. The overlap population (Table 4) of bond C2−C4 (0.591) is larger than that of C4−C5 (0.541), which agrees with the fact that the bond length C2−C4 (1.376 Å) is shorter than that of C4−C5 (1.421 Å) of C_4H_5N. The relation between the bond length and the bond overlap population is that the larger the overlap population, the shorter the bond length. Above all, the bond length and the overlap population indicate that both C2−C4 and C3−C5 have relatively double bond character and the bond C4−C5 has relatively single bond character. However, these double and single bonds are not the same as those in the common interests. These single bonds are slightly shorter than the common single bond, and these double bonds are slightly longer than the common ones. Obviously, this observation should be attributed to the conjugation effect.

The bond lengths (Å), bond angles (deg), and rotational constants (GHz) of pyrrole cation calculated by MP2(full), B3P86, B3LYP, and B3PW91 methods using 6-31G* and 6-311+G* basis sets are given in Table 2. The bond angles calculated with the two basis sets are found to be approximately equal to each other. The results of the three DFT methods are in good agreement with the ab initio method (MP2(full)) ones.

From Table 2 it can be seen that pyrrole cation is also of C_{2v} symmetry in the gas phase and all of the atoms are located in a plane. Pyrrole cation is also a compound of five-membered

TABLE 3: Computed Major Bond Lengths (Å), Bond Angles (deg), Dihedral Angles (deg), Rotational Constants (GHz), and Zero-Point Vibrational Energies (kcal/mol) of Complex 1, Complex 2, and Complex 3 Using 6-31G* Basis Set

	complex 1			complex 2			complex 3	
	B3P86	B3LYP	B3PW91	B3P86	B3LYP	B3PW91	B3P86	B3LYP
				Bond Lengths				
C3−C13	2.754	2.859	2.754					
C3−C12				2.727	2.924	2.795		
N1−H16							2.362	2.741
N1−C2/N11−C12	1.363	1.370	1.364	1.363	1.700	1.365	1.369/1.370	1.369/1.372
N1−C3/N11−C13	1.359	1.364	1.360	1.365	1.370	1.365	1.369/1.349	1.369/1.360
C2−C4/C12−C14	1.399	1.402	1.400	1.396	1.401	1.397	1.392/1.408	1.397/1.412
C3−C5/C13−C15	1.412	1.414	1.413	1.411	1.414	1.413	1.392/1.420	1.397/1.419
C4−C5/C14−C15	1.394	1.398	1.395	1.394	1.400	1.396	1.410/1.384	1.414/1.389
N1−H6/N11−H16	1.010	1.011	1.010	1.011	1.012	1.011	1.011/1.013	1.011/1.019
				Bond Angles				
N1−C3−C13	96.5	97.3	97.1					
N1−C3−C12				105.9	106.8	106.7		
C5−C3−C13	92.7	91.2	88.7					
C5−C3−C12				88.4	87.8	87.6		
C2−N1−C3/ C12−N11−C13	109.8	109.7	109.8	109.8	109.7	109.8	109.7/109.3	110.0/109.0
N1−C2−C4/ N11−C12−C14	108.2	108.1	108.2	108.3	108.2	108.3	107.8/108.2	107.8/108.3
N1−C3−C5/ N11−C13−C15	107.5	107.5	107.5	107.2	107.3	107.3	107.8/108.1	107.8/108.3
H6−N1−C2/H16−N11−C12	125.1	125.2	125.1	125.0	125.0	125.0	124.9/123.7	125.0/124.8
N1−C2−H7/ N11−C12−H17	121.3	121.3	121.3	121.3	121.3	121.3	121.4/120.9	121.5/121.4
N1−C3−H8/ N11−C13−H18	121.6	121.6	121.6	121.7	121.6	121.7	121.4/122.0	121.5/121.7
C2−C4−H9/ C12−C14−H19	125.4	125.4	125.4	125.4	125.4	125.4	125.2/125.3	125.1/125.2
C3−C5−H10/ C13−C15−H20	125.1	125.1	125.1	125.0	125.1	125.1	125.2/125.0	125.1/125.1
				Dihedral Angles				
C2−N1−C3−C13	91.3	92.2	91.6	−97.3	−96.7	−92.1		
H8−C3−N1−C2	171.9	173.5	172.2	−172.7	−174.0	−172.8	177.6	178.7
H18−C13−N11−C12	171.9	173.5	172.2	−172.7	−174.0	−172.8	180.0	180.0
				Rotational Constants				
A	3.201	3.153	3.184	2.545	2.477	2.528	3.120	3.370
B	0.799	0.759	0.780	1.084	1.028	1.060	0.667	0.527
C	0.720	0.687	0.704	1.051	1.067	1.031	0.624	0.505
				Zero-Point Vibrational Energies				
	105.37	104.70	105.18	105.54	104.81	105.37	104.35	103.95

TABLE 4: Mulliken Population Analysis for the Total Atomic Charges and the Bond Overlap Populations of C_4H_5N, $C_4H_5N^+$, Complex 1, Complex 2, and Complex 3 at the B3P86/6-31G* Level

	C_4H_5N	$C_4H_5N^+$	complex 1	complex 2	complex 3
			Total Atomic Charges		
N1/N11	−0.581	−0.553	−0.532/−0.532	−0.558/−0.558	−0.566/−0.564
C2/C12	0.003	0.135	0.046/ 0.046	0.059/ 0.059	0.008/ 0.087
C3/C13	0.003	0.135	0.023/ 0.023	0.039/ 0.039	0.008/ 0.092
C4/C14	−0.214	−0.161	−0.207/−0.207	−0.192/−0.192	−0.224/−0.178
C5/C15	−0.214	−0.161	−0.187/−0.187	−0.197/−0.197	−0.224/−0.178
H6/H16	0.353	0.437	0.398/ 0.398	0.401/ 0.401	0.397/ 0.417
			Overlap Populations		
C3−C13			0.030		
C2−C13				0.031	
N1−C2/N11−C12	0.374	0.370	0.376/0.376	0.374/0.374	0.368/0.375
N1−C3/N11−C13	0.374	0.370	0.379/0.379	0.366/0.366	0.368/0.383
C2−C4/C12−C14	0.591	0.479	0.541/0.541	0.547/0.547	0.561/0.502
C3−C5/C13−C15	0.591	0.479	0.512/0.512	0.511/0.511	0.561/0.489
C4−C5/C14−C15	0.541	0.592	0.567/0.567	0.566/0.566	0.541/0.567
N1−H6/N11−H16	0.324	0.314	0.319/0.319	0.321/0.321	0.322/0.296

heterocyclic aromatic ring, which is the same as the structure of pyrrole. The differences in the bond angles between pyrrole and its cation are no more apparent than those of the bond lengths. The bond distances of N1−C2 are similar in both pyrrole (1.370 Å) and pyrrole cation (1.359 Å), by revealing the slight difference of 0.011 Å. The distinct difference of pyrrole and pyrrole cation lies in the bond lengths between C2−C4/C3−C5 and C4−C5 bonds. In pyrrole, the bond length C2−C4/C3−C5 (1.376 Å) is shorter than that of C4−C5 (1.421 Å), but in pyrrole cation, the bond length C2−C4/C3−C5 (1.430 Å) is longer than the bond length C4−C5 (1.371 Å). As mentioned above, in pyrrole, C2−C4 and C3−C5 have the double bond character, while the C4−C5 has a single character. But in pyrrole cation, they are inverse, C4−C5 (1.371 Å) is shorter than that of C2−C4/C3−C5 (1.430 Å). This theoretical prediction indicates that adding or removing an electron may effectively change C2−C4/C3−C5 and C4−C5 bonding characters. The overlap population of C4−C5 (0.592) for the pyrrole cation, being larger than that of C2−C4/C3−C5 (0.479), also proves that the larger overlap populations between the bonds are well correlated with the corresponding shorter bond. Above all, the bond length and the overlap population indicate that the C2−C4/C3−C5 bond length is longer than the C4−C5 bond length for pyrrole cation. In addition, it should be noted that

the other bonds, such as the N−H and C−H bonds, are basically unchanged for the two systems.

The vibrational frequencies have also been determined for pyrrole using MP2(full) and DFT (B3P86, B3LYP, and BLYP) methods with 6-31G* and 6-311+G* basis sets, the results, together with the corresponding experimental data, are given in the Supporting Information (see Table S1). It is shown that pyrrole molecule includes 24 fundamental symmetries, 9 a_1, 3 a_2, 4 b_1, and 8 b_2. The calculations using the 6-311+G* basis set at the same level give the results in slightly better agreement with the experimental data than those using the 6-31G* basis set. For the given basis set 6-31G* or 6-311+G*, the B3LYP and BLYP results are very close to experimental ones. MP2 results are slightly larger than the experimental values. So we choose B3LYP and BLYP levels with 6-31G* and 6-311+G* basis sets to calculate the vibrational frequencies of pyrrole cation. Considering the computer CPU time and disk space, the B3LYP and BLYP methods with 6-31G* basis set are chosen to calculate the vibrational frequencies of dimeric cations (three complexes).

Table 4 shows that pyrrole cation also includes 24 fundamental symmetries (9 a_1, 3 a_2, 4 b_1, 8 b_2) as pyrrole does, but the vibrational frequencies of pyrrole cation are lower than the corresponding frequencies of pyrrole with the exception of some a_2 symmetries. As to the a_1 symmetries, the nine vibrational frequencies (cm^{-1}) in pyrrole calculated with the B3LYP DFT method are 3697, 3300, 3279, 1530, 1454, 1194, 1110, 1051, and 900 cm^{-1}. The nine vibrational frequencies having the same symmetry in pyrrole cation are 3605, 3298, 3282, 1563, 1476, 1181, 1106, 1084, and 895 cm^{-1}, respectively. Obviously, the former three frequencies for each species correspond to the N−H and C−H in-plane stretching vibrations, the middle three correspond to the C−N and C−C in-plane stretching vibrations, while the last three denote the in-pane bending vibrations of C−H, C−C, and C−N bonds. By removing an electron from the pyrrole, the in-plane H−N stretching vibration is red-shifted by 92 cm^{-1}, the IR intensity also indicates that this mode corresponds to an apparent absorption peak. The in-plane C−N, one C−C stretching, and one C−H in-plane bending vibrations are blue-shifted by 20−30 cm^{-1}; another in-plane C−C stretching mode is slightly red-shifted, but these absorptions are very weak. The remaining other a_1 modes are basically unchanged. Three a_2 modes lie in the range of 500−900 cm^{-1} and denote the out-of-plane bending vibrations. But, they are IR-spectroscopically invisible, viz., no absorption peak exists. The four b_1 modes denote the out-of-plane bending vibrations of C−H and C−C bonds and they are blue-shifted by 11−72 cm^{-1} also with the weak absorptions if removing an electron from pyrrole. In the left eight b_2 modes for the pyrrole, the visible absorption peak corresponds to the coupling motion between the in-plane N−H bending and the out-of-plane C−N bending, its red shift is about 100 cm^{-1} after removing an electron. From this analysis, it can be known that regardless of the oxidation of the pyrrole or the reduction of the pyrrole cation, there are three major visible IR signals that correspond to the N−H stretching (3605−3697 cm^{-1}), the C−C/C−N stretching (1505−1606 cm^{-1}), and out-of-plane C−H bending (732−743 cm^{-1}) vibrations.

4.2. Three Encounter Complexes. Formation of the encounter complex, also termed as precursor complex, is the first stage of the ET reaction. The geometrical configuration of the encounter complex influences directly not only the activation energy of reaction but also the ET coupling matrix element and further the ET rate. Thus it is very important to find various possible geometrical configurations for the encounter complex. In this paper, three stable encounter complexes have been found by using DFT methods with the 6-31G* basis set. Obviously, these stable encounter complexes only correspond to three different situations which represent three different coupling modes when the reacting system is in its stable states. For convenience, three stable encounter complexes are expressed as complex 1, complex 2, and complex 3. The equilibrium geometry of complex 3 is different from those of the other two former complexes. The calculated vibrational frequencies (cm^{-1}) and IR intensities (km/mol) of three complexes are listed in the Supporting Information (see Table S3).

The equilibrium bond lengths (Å), bond angle (deg), dihedral angle (deg), rotational constant (GHz), and zero-point vibrational energy (kcal/mol) of the three complexes formed between neutral pyrrole and its cation are given in Table 3. The calculations indicate that three complexes have C_1 symmetry in gas phase, and they are all composed of two rings. The two rings of each complex are different from that in the monomer, namely, all of the atoms of each ring do not lie in the same plane, with the exception of one ring of complex 3. The one ring (all of the atoms of the ring lie in a plane) of complex 3 has C_{2v} symmetry. The differences of bond angles among three complexes are small relative to those of the pyrrole monomer and its cation. In complex 1, the biggest distortion of all atoms is H8 or H18, and the dihedral angles of H8−C3−N1−C2 or H18−C13−N11−C12 are 171.9°, 173.5°, and 172.2° at B3P86, B3LYP, and B3PW91 levels, respectively. The same phenomenon can be observed in complex 2 where the biggest distortion of all atoms is H8/H18 and the dihedral angles of H8−C3−N1−C2 or H18−C13−N11−C12 are −172.7°, −174.0°, and −172.8° at B3P86, B3LYP, and B3PW91 levels, respectively. As to complex 3, the dihedral angle of (H6−N1−C2−C4) is −173.6° at the B3P86 level.

In complex 1, the nearest two atoms that belong to two rings are C3 and C13. The distances of C3−C13 are 2.715 Å, 2.859 Å, and 2.754 Å using B3P86, B3LYP, and B3PW91, respectively. The N1−N11 distances of complex 1 are 3.194 Å, 3.373 Å, and 3.255 Å by using the three DFT methods, respectively. The bond lengths of C4−C5/C14−C15 (1.394 Å) in complex 1 are shorter than that of C3−C5/C13−C15 (1.412 Å) using the B3P86/6-31G* method. Compared with those of the monomers, these bond lengths in complex 1 tend to the averaged ones. In particular, the C3−C5/C13−C15 or C2−C4/C12−C14 bonds are longer than those of the corresponding C2−C4 or C3−C5 of the pyrrole, and shorter than those of those of the pyrrole cation. The C4−C5/C14−C15 bonds are also between those of pyrrole and pyrrole cation. Obviously, the double and single bonds are indistinguishable for this complex. The overlap populations of C4−C5/C14−C15 and C3−C5/C13−C15 are 0.567 and 0.512, and the bond lengths are 1.394 Å and 1.412 Å, respectively. These data have also proved the above analysis. But for all C−H and N−H bonds, they are basically unchanged before and after forming the complex.

In complex 2 the nearest two atoms that belong to two rings are C3 and C12. The distance of C3−C12 is 2.727 Å, 2.924 Å, and 2.795 Å at B3P86, B3LYP, and B3PW91 levels, respectively. The two N atoms in two rings are not directly contacted, so their interatomic distance is longer, compared with that in complex 1, being 4.355 Å, 4.548 Å, and 4.534 Å at the given levels. All other bond lengths are very close to the corresponding bond lengths of complex 1, indicating that the bonding character of complex 2 is similar to that in complex 1. In complex 2 the overlap population of C4−C5/C14−C15 (0.566) is slightly larger than, but very close to that, of C3−C5/C13−C15 (0.511),

TABLE 5: Total Energies (a.u.) of C_4H_5N, $C_4H_5N^+$, Complex 1, Complex 2, and Complex 3 and the Stability Energies (ΔE, kcal/mol) of Complex 1, Complex 2, and Complex 3

	6-31G*			6-311+G*		
	B3P86	B3PW91	B3LYP	B3P86	B3PW91	B3LYP
C_4H_5N	−210.8168268	−210.0888306	−210.1658902	−210.8656478	−210.1366624	−210.2192529
$C_4H_5N^+$	−210.5068702	−209.7997520	−209.8793433	−210.5476342	−209.8397000	−209.9224705
complex 1	−421.3631092	−419.9253196	−420.0827423	−421.4506286	−420.0108923	−420.1758838
complex 2	−421.3612254	−419.9239900	−420.0816549	−421.4481907	−420.0090558	−420.1739528
complex 3	−421.3507981	−419.9141069	−420.0738114	−421.4384934	−419.9999200	−420.1671206
ΔE_1	24.73	23.05	23.54	23.43	21.67	21.44
ΔE_2	23.51	22.18	22.82	21.87	20.48	20.19
ΔE_3	16.98	15.99	17.90	15.79	14.76	15.91

being consistent with the fact that the bond length of C4−C5/C14−C15 (1.394 Å) is slightly shorter than the bond length of C3−C5/C13−C15 (1.411 Å). But in brief, the difference between the double and single bonds is not notable.

In complex 3 the nearest two atoms in two rings are N1 and H16, their distance is 2.623 Å obtained by using the B3P86/6-31G* method. One ring of complex 3 has the C_{2v} symmetry and another pyrrole ring lies vertically over this ring, contacting the H of the N−H with the N atom of the first ring. In the second ring, all atoms are coplanar. The character of bonds in complex 3 is different from that in complex 1 and complex 2. In the ring that has the C_{2v} symmetry, the bond C2−C4/C3−C5 (1.392 Å) is shorter than the bond C4−C5 (1.410 Å), which is similar to the structure of the pyrrole. But the bond lengths have also a tendency to the averaged ones. The overlap population (Table 4) of bond C2−C4/C3−C5 (0.561), being slightly larger than but also very close to that of C4−C5 (0.541), has also provided evidence for the fact that the bond length C2−C4/C3−C5 (1.392 Å) is very close to that of the C4−C5 (1.410 Å) length of C_4H_5N. The C14−C15 (1.384 Å) is shorter than that of C12−C14 (1.408 Å) and C13−C15 (1.420 Å). The overlap populations of C14−C15, C12−C14, and C13−C15 are 0.567, 0.502, and 0.489, respectively, which agree with the relation between bond overlap population and bond length. Similarly, changes in all C−H and N−H bond lengths are very small.

The Mulliken population analysis for the total atomic charges indicate that the N atoms of C_4H_5N, $C_4H_5N^+$, complex 1, complex 2, and complex 3 gain approximately 0.58, 0.55, 0.53, 0.56, and 0.57 electrons, respectively, at the B3P8/6-31G* level. These electrons are withdrawn from the neighboring C atoms and the H atoms to the N atoms.

4.3. Relative Stability of the Coupling Complexes. Table 5 shows the energies of C_4H_5N, $C_4H_5N^+$, complex 1, complex 2, and complex 3 and the stabilization energies of the three complexes. It is well-known that the lower the total energy of the complex is, the more stable it is. That is to say that the larger the stabilization energy is, the more stable it is. At the B3P86/6-31G* level, the stabilization energies of complex 1, complex 2, and complex 3 are 24.73, 23.51, and 16.98 kcal/mol, respectively. At the B3P86/6-311+G* level, they become 23.43, 21.87, and 15.79 kcal/mol, respectively. These data have clearly indicated the order of the stability of the three complexes to be that complex 1 > complex 2 > complex 3.

With the correction for basis set superposition error (BSSE), the stabilization energies of complex 1, complex 2, and complex 3 are 23.94, 22.83, and 16.58 kcal/mol, respectively, at the B3P86/6-31G* level; the stabilization energies decrease by 0.79, 0.68, and 0.40, respectively, relative to those without the correction for BSSE. Using the correction for BSSE, the stabilization energies of complex 1, complex 2, and complex 3 at the B3LYP/6-31G* level are 23.21, 22.80, and 16.41 kcal/mol, respectively. At the B3PW91/6-31G* level, the values are 21.72, 21.88, and 13.64 kcal/mol, respectively. These results have indicated that for the three complexes the correction for BSSE cannot significantly change the stabilization energy values, and also do not change the stability order of the complexes. Overall, the stability of the three complexes is in the order: complex 1 > complex 2 > complex 3.

Frequency analysis (see Table S3 in Supporting Information) shows that there are not any imaginary frequencies for complex 1 and complex 2. But for complex 3, there are two small imaginary vibrational frequencies (68i cm^{-1} and 42i cm^{-1}) using the B3P86 method and one small imaginary vibrational frequency (22i cm^{-1}) using the B3LYP method with the 6-31G* basis set. This observation indicates that complex 1 and complex 2 are really the stable minima on the global potential energy surface, and that complex 3 may be a metastable state. This is because the potential energy surface in that zone corresponding to complex 3 is more flat, some slight geometrical constraint by the surrounding may cause the system to be unrelaxed completely. Inspection of the imaginary frequency modes reveals that at the B3P86/6-31G* level the first imaginary frequency mode corresponds to the swing of the above ring departing from the C_s symmetry plane, while the second one corresponds to the rolling of the above ring relating to another ring. Obviously, the swing of the above ring may favor the isomerizations into complex 1 or 2, whereas the rolling of the above ring may favor the increase of the interaction between two rings while keeping the coupling mode unchanged. However, the very small absolute values of these imaginary frequencies have implied a small possibility of isomerizing into the other complexes (1 or 2). So it may be considered as a metastable state. Actually this case may be observed frequently in biological systems: the peptide chain, DNA chain, and the amino acid residues may restrict their terminal active sites or groups so as not to contact with the other active sites linked to the other biological molecular chains or the amino acid residues with the optimum coupling mode. Although perhaps there are some restrictions between arbitrary active sites or groups, there are still some interactions between them. This interaction may make the system slightly more stable than that in their separated state and further provide a condition for favoring the ET and the proton transfer or the other reaction processes. Therefore, the discussion about this kind of structure is also necessary for further exploring the interaction mechanism and the coupling modes for the systems at some nonequilibrium states.

5. ET Kinetics Parameters

The structural character and the relative stability of three stable encounter complexes and their monomers have been discussed above. However, the ET is not limited to occurring at the optimum complex geometry. It may take place not only

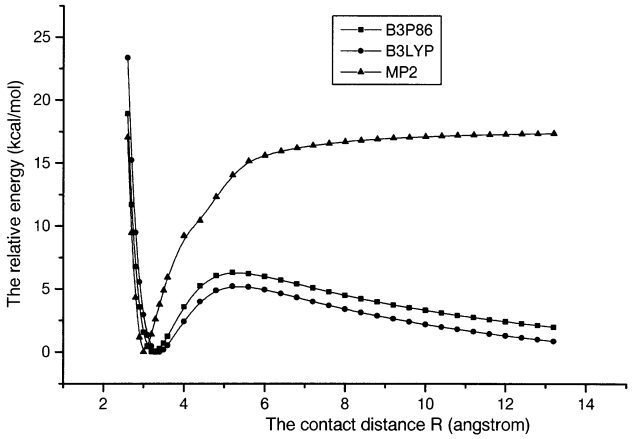

Figure 3. Dependences of the relative energies of the coupling system at the activated state via coupling mode 1 on the contact distance $R_{(C3-C13)}$ (Å). For each curve, the minimum energy is taken as the energy zero point. This note also applies to Figures 4 and 5.

at different contact distances but also at different orientations. Therefore it is very helpful to expand the three stable encounter complexes to different coupling modes for exploring the overall ET reactivity of this system. Actually these stable states do not denote the states in which the electron transfer is more likely to take place. Only when the structural activation and reorganization make the system satisfy the energy conservation before and after the electron transfer may the electron transfer occur. This indicates that it is key to the electron transfer to yield the suitable activated state with the energy conservation, but it is not important from where the activated state is produced. However, different initial states may yield different activated states. The optimized three stable encounter complexes have implied the three different initial coupling modes that are favorable to the electron transfer. So on the basis of these three stable encounter complexes, it is helpful to design three different coupling modes to the exploration of the electron transfer reactivity. On the basis of the above definitions for three coupling modes, the contact distance dependences of the relevant ET kinetics parameters will be explored in the following sections.

5.1. Energy Curves. To explore the correct dissociation behavior and to demonstrate the suitability of computational methods and basis sets, the potential energy surfaces of the reacting system $[C_4H_5N\cdots C_4H_5N^+]$ for the dissociation processes via the three different modes, which are closely related to the three stable encounter complexes, have been first scanned. In the scanning, the contact distance R_{a-b} is changed, the relative orientation of two rings in the complex is fixed, and all other parameters are optimized. Accordingly, the defined three coupling modes are viewed as coupling mode 1, coupling mode 2, and coupling mode 3; the defined contact distances for three coupling modes have been displayed in Figure 2 and they are C3−C13 (coupling mode 1), C3−C12 (coupling mode 2), and N1−H16 (coupling mode 3) bond distances, respectively. They are referred to the distance between two nearest atoms in two rings. Figures 3−5 show the scanned energy curves of three encounter complexes with different contact distances R_{a-b} by constraining the relative orientation and relaxing the other bond lengths. In Figures 3−5, the minimum energy at the optimum contact distance where R_{a-b} is about 2 Å is defined as zero point for every coupling mode.

From Figures 3−5 it can be seen that the energy curves with the DFT methods (B3LYP, B3P86) exhibit abnormal behavior. This abnormal behavior was first reported in an important paper

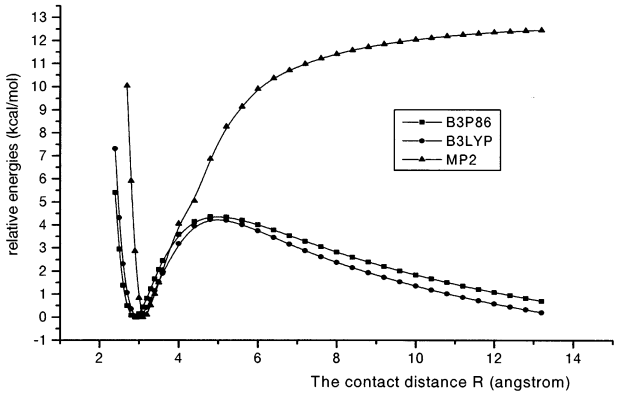

Figure 4. Dependences of the relative energies of the coupling system at the activated state via coupling mode 2 on the contact distance $R_{(C3-C12)}$ (Å).

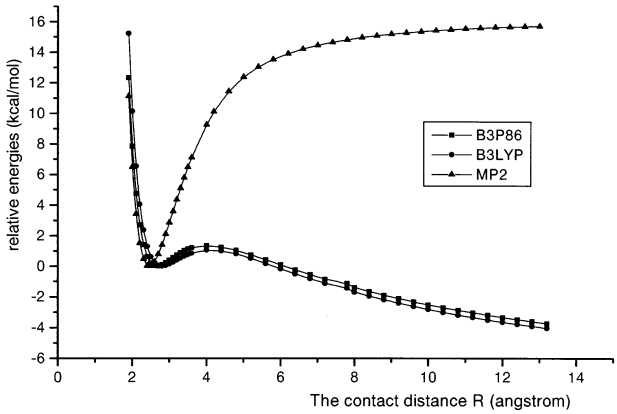

Figure 5. Dependences of the relative energies of the coupling system at the activated state via coupling mode 3 on the contact distance $R_{(N1-H16)}$ (Å).

by Bally and Sastry in 1997,[28] and it was named "inverse symmetry breaking". Lately the "inverse symmetry breaking" problem was mentioned[28,29] as a common phenomenon for the DFT results for radical ion with two equivalent fragments.

The abnormal behavior of DFT methods can be depicted from the following two aspects. One is that the larger the contact distance, the lower the energy. That is to say, in the process of scanning the energies of three complexes at the activated states, (even though there exist minima on their energy curves) when R_{a-b} increases from the lowest energy state, the energy calculated by DFT methods increases first, but after surmounting a fictitious transition state barrier, it decreases. The other abnormal behavior is that regardless of the contact distance, the positive charge and the spin of the three radical cations are delocalized evenly at the two fragments. In fact, it should be such a case that when R_{a-b} is large enough, the total energy of each complex is the sum of the total energies of its monomers, C_4H_5N, and $C_4H_5N^+$, and the positive charge and the spin density of each complex cation are not delocalized evenly at the two fragments. So the results of energy curves with DFT methods are definitely unreasonable. However, as to the MP2 method, the energy curves exhibit normal behavior. Along with the increases of the contact distance from 2 to 13 Å, the energy of the system decreases first, but after passing a minimum value, it increases until the dissociation limit. This is obviously reasonable. So the MP2 method has been chosen to scan the energy curves of the three complexes at the activated states in order to calculate the ET rates of the $C_4H_5N/C_4H_5N^+$ system at the different contact distances.

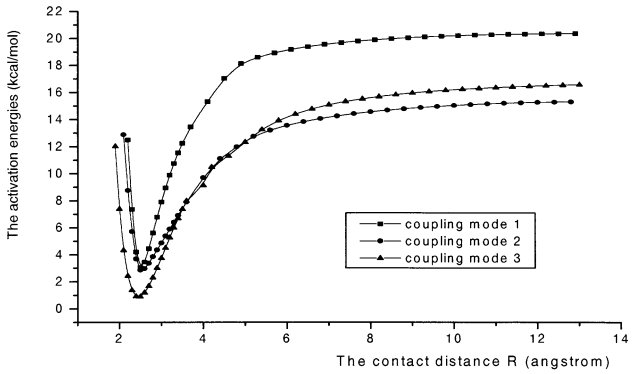

Figure 6. Contact distance R_{a-b} (Å) dependence of the activation energy $E_a(R_{a-b})$ (kcal/mol) via the three coupling modes.

Similarly, in the scan optimization for the activated states according to the three different coupling modes, the relative orientations of two rings are constrained for each coupling mode, all other geometrical parameters are optimized when changing the contact distance. So the potential energy surfaces have been obtained for the activated states.

5.2. Activation Energy. Activation energy is the energy barrier of the ET reaction. The larger the activation energy, the more difficult the ET reaction. From eq 9, it can be seen that the ET rate and the activation energy exhibit as an exponential relation.

The dependence of activation energy $E_a(R_{a-b})$ on the contact distance R_{a-b} has been demonstrated in Figure 6. At the present time, no experimental activation energy has been reported for this kind of ET reaction. From Figure 6 it can be seen that the activation energies via three different coupling modes exhibit same characteristic variety. Actually, these observed variety regularities for the activation energy should be attributed to the changes of C2−C4/C3−C5 and C4−C5 bonds. Comparing the geometrical parameters of pyrrole and pyrrole cation, it can be known that the substantial changes in the reactant geometries should be those of the C2−C4/C3−C5 and C4−C5 bonds before and after ET. For pyrrole, before ET, the C2−C4 and C3−C5 have the double-bond character, while the C4−C5 has the single-bond character. However, after ET, the C2−C4 and C3−C5 bonds become of the single bond property, and the C4−C5 bond becomes of the double bond property. All other geometrical parameters (bond lengths and bond angles) are almost unchanged. Obviously, this observation has indicated that ET may significantly change the C2−C4/C3−C5 and C4−C5 bonds. Therefore, in the activation process for each definite coupling mode, the activation of the system is mainly referred to the C2−C4/C3−C5 and C4−C5 bond length changes. Namely, the energy increase of the system due to the C2−C4/C3−C5 and C4−C5 bond length changes consists of the main contribution to the total activation energy. At the activated states, these three bonds become as the averaged ones.

For the nonadiabatic process in which the donor and the acceptor lie in the infinite separated state, no coupling interaction between them exists. On the basis of eq 13, selecting C2−C4/C3−C5 and C4−C5 as variables and fixing the other parameters as constants (because they are almost unchanged in ET process, they may be set to be averaged values between in pyrrole and in pyrrole cation), the potential energy surface at the activated state can be obtained, and further the activated parameters can be determined by the minimization method. The obtained activated parameters are 1.404 Å (C2−C4/C3−C5), 1.398 Å (C4−C5), 1.364 Å (N1−C2/N1−C4), 1.010 Å (N1−H), and 1.08 Å (C−H) at the B3P86/6-31G* level. Obviously, these activated parameters are almost equal to the averaged values of the corresponding bond lengths in two monomers (C2−C4/C3−C5 = 1.403 Å, C4−C5 = 1.396 Å, N1−C2/N1−C4 = 1.365 Å at the same theoretical level). As a good approximation, the activation energy curve can be obtained according to eq 14 and by fixing these activated parameters in the scanning R_{a-b} dependence of E_a. It should be noted that the geometrical parameters in the encounter complexes also depend on the contact distance, R_{a-b}. For two limit cases, they are tendency to those in isolated monomers when R_{a-b} is infinite, while they are close to those of the stable encounter complexes when R_{a-b} becomes small. Only the geometrical parameters for these two limit cases have been given in Tables 1−3. All the other parameter values are between those in these two limit cases.

From Figure 6, it can be known that when the contact distance increases, the activation energy deceases first, but after passing a minimum activation energy barrier, it increases. In detail, as for the ET reaction via the coupling mode 1, when the contact distance is 2.2 Å, the activation energy is 12.48 kcal/mol. With the contact distance increasing, the activation energy decreases sharply. When the contact distance is 2.5 Å, the activation energy is only 3.04 kcal/mol. As the contact distance continuously increases from 2.5 to 13.0 Å, the activation energy increases continuously. When $R_{a-b} > 6.0$ Å, the value of activation energy has increased by about 10 times the minimum value. As for the ET reaction via coupling mode 2 and coupling mode 3, the variation tendencies are the same as that in the ET reaction via coupling mode 1. For coupling modes 2 and 3, the minimum activation energies are 2.85 kcal/mol and 0.91 kcal/mol, respectively, where contact distance is 2.5 Å. The minimum activation energies via the three coupling modes are in the order coupling mode 1 > coupling mode 2 > coupling mode 3.

Comparison among the activation energy curves of three coupling modes can give a relative standard for predicting the ET reactivity at different contact distances. From Figure 6 it can be known that in all of the contact distances, the activation energies for the three coupling modes have the same change tendency, only the activation energy curve for coupling mode 3 is slightly lower by ~2 kcal/mol than that for coupling modes 1 and 2, and all of them are almost coincided. Thus from the viewpoint of the activation energy, it can be predicted that the most favorable coupling mode for ET should be coupling mode 3.

5.3. Coupling Matrix Element. Equation 7 implies that the ET rate strongly depends on the coupling matrix element. The larger the coupling matrix element, the faster the rate of ET. The dependence of the coupling matrix element H_{if} on the contact distance R_{a-b} has been demonstrated in Figure 7 and the corresponding results are also given in Tables S4a and S4b in the Supporting Information. From Figure 7 it can be known that the coupling matrix elements via the three different coupling modes also exhibit the same characteristic variety. When the contact distance increases, the coupling matrix element increases first, and after surmounting a maximum, it decreases along with the increase of contact distance. As for ET reaction via the coupling mode 1, when the contact distance is 2.2 Å, the coupling matrix element is 9.62 kcal/mol. With the contact distance increasing, the coupling matrix element increases sharply. When the contact distance is 2.5 Å, the coupling matrix element is 19.06 kcal/mol, reaching the maximum. For the other contact distances going from 2.5 to 13.0 Å, the coupling matrix elements decrease monotonically. In the range of 2.2 Å < R_{C3-C13} < 6.0 Å, H_{if} changes rapidly and the values of H_{if} in the range of the above contact distance are greater than those

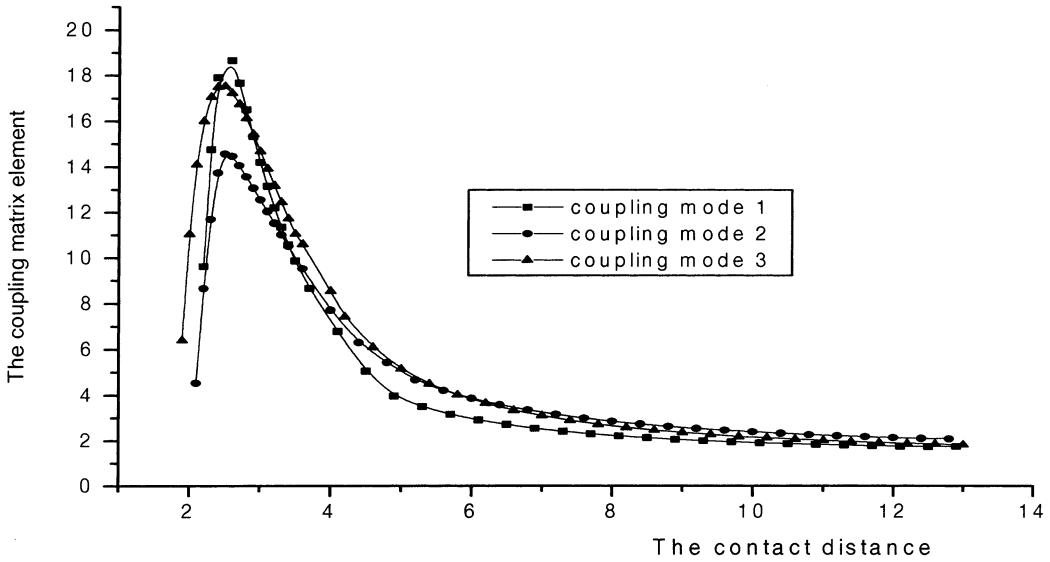

Figure 7. Contact distance R_{a-b} (Å) dependence of the coupling matrix element $H_{if}(R_{a-b})$ (kcal/mol) via the three coupling modes.

in the other contact distances. So a conclusion can be drawn that in the range from 2.2 to 6.0 Å, the coupling effect of the donor and the acceptor is strong, which is the major zone of the ET reaction. As for the ET reaction via coupling mode 2 and coupling mode 3, the variation tendencies of the coupling matrix elements are the same as those via the coupling mode 1.

Analogously, if one analyzes the curve change regularity by comparing them at the same the contact distance, one can distinguish which coupling mode is more favorable to the ET. From Figure 7, it can be seen that three coupling modes basically have same change tendency. At the infinite contact distance, three curves basically coincide as one. This is obviously reasonable, because at this position, the orbital overlap between the donor and the acceptor is too small, and the orientation effect is also not significant, only the electrostatics interaction between the donor and the acceptor plays some role in the coupling, which is similar to the classical dipole−dipole interaction. When $R_{a-b} < 2.5$ Å, the curves of the three modes sharply decrease along with the decrease of R_{a-b}. In the range 2.2 Å $< R_{a-b} <$ 3.5 Å, coupling mode 1 has the largest H_{if}, which is more favorable to the ET compared with the other two modes. Mode 3 is the next, and mode 2 is smaller than mode 3.

These curve regularities can be interpreted by the detailed comparison regarding the contact cases of the three coupling modes. For coupling mode 1, it is the direct face−face contact of two rings. Obviously, this mode favors the $\pi-\pi$ molecular orbital direct interaction between two rings, and all p_π-type orbitals of all atoms may participate in the coupling. So this mode should have the strongest coupling interaction. But for coupling mode 2, although it is the parallel coupling, similar to the coupling mode 1, it has the contact between two rings only by a part of atoms, being the edge−edge contact. This is to say that only a part of the p_π-type orbitals interact with each other. Compared with coupling mode 1, coupling mode 2 is apparently much weaker. However, for coupling mode 3, the N−H of one ring directly interacts with the N site by vertical mode to form an N−H···N hydrogen bond. Although this mode also has few direct interacting atoms (only one for each ring), it avoids the large repulsion interaction between two rings and makes the H atom in H−N easily approach to the N atom in another ring. In the stable encounter complex, the shortest contact distance (N1−H16) in the complex 3 is 2.632 Å at B3P86/6-31G* level, it is considerably smaller than those distances (2.751 Å for C3−C13 in complex 1 and 2.727 Å for C3−C12 in complex 2) in the other two complexes. Obviously the smaller contact distance makes the coupling interaction in coupling mode 3 stronger than that in mode 2.

In the shorter range of contact distance, the coupling matrix elements in three coupling modes exhibit relative regularity similar to those in the three stable encounter complexes. However, the coupling matrix elements in the three coupling modes have different variation rates along with the increase of the contact distance. For the H-bond coupling mode (coupling mode 3), since the direct interacting atoms are few (only two), along with the increase of the contact distance, the decrease of the coupling interaction should be more sharp than that in coupling mode 2 with a similar interaction situation. But for mode 1, since the interacting area between two rings is significantly larger than that in the other two modes, the decrease rate should be larger than in modes 2 and 3 as the contact distance increases. Figure 7 has clearly demonstrated the analysis.

5.4. ET Rate. Equation 7 shows that there are two contributions to the ET rate $k_{et}(R_{a-b})$. They are the coupling matrix element $H_{if}(R_{a-b})$ and the Franck−Condon factor FC(R_{a-b}). The FC factor depends on activation energy $E_a(R_{a-b})$ and reorganization energy $E_\lambda(R_{a-b})$. As to the self-exchange ET reaction, the Marcus approximate relation told us that the activation energy $E_a(R_{a-b})$ equals to a quarter of the reorganization energy $E_\lambda(R_{a-b})$ under the harmonic approximation. Strictly, this approximate relation does not pledge to work well for any systems. The anharmonic correction becomes necessary, especially for the systems with large geometrical changes before and after ET and with strong initial−final state coupling interactions.[16,20,30−32] Calculations have indicated for this kind of systems that the ET potential energy surfaces are harmonic, so it can be predicted to give reasonable results. In particular, when the contact distance increases, the coupling interaction between initial and final states gradually becomes smaller and smaller, and the ET potential energy surface becomes much more harmonic, and the anharmonic effect may be negligible. Therefore, it may be said that the ET rate of different contact distance depends strongly on the activation energy $E_a(R_{a-b})$ and coupling matrix element $H_{if}(R_{a-b})$. The contact distance R_{a-b}(Å) dependence of the electron transfer rate $\log(k_{et}(R_{a-b}))$ via the three coupling

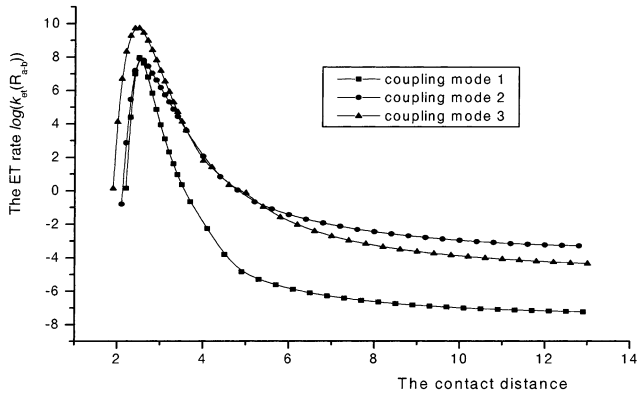

Figure 8. Contact distance R_{a-b} (Å) dependence of the electron-transfer rate $\log(k_{et}(R_{a-b}))$ via the three coupling modes.

modes has also been shown in Figure 8. From the factors that influence the ET rate and Figure 8, it can be seen that in the range of the contact distance going from about 2.0 to 13.0 Å, the rate of ET increases at first, after arriving at the maximum, then decreases at last. As to the ET reaction via the coupling mode 1, the rate of ET tends to the maximum constant value (7.75×10^7 s^{-1}) where the contact distance R_{C3-C13} is about to 2.5 Å, and the system has the lowest activation energy (3.04 kcal/mol) and the biggest coupling matrix element (19.06 kcal/mol). After 2.5 Å of the contact distance, k_{et} rapidly decreases along with R_{C3-C13} increase. When $R_{C3-C13} > 6.0$ Å, k_{et} decays gently along with the increase of contact distance, and the system has larger activation energy and smaller coupling matrix element. When $R_{C3-C13} > 6.0$ Å, k_{et} has decreased by about twelve orders of magnitude. As to the ET reaction via coupling mode 2, k_{et} tends to the maximum value (9.37×10^7 s^{-1}) where R_{C3-C12} is about 2.5 Å. At this state, the system has the lowest activation energy (2.85 kcal/mol) and the largest coupling matrix element (14.56 kcal/mol). As to the ET reaction via coupling mode 3, k_{et} tends to the maximum value (5.27×10^9 s^{-1}) where R_{N1-H16} is also about 2.5 Å. With the increase of contact distance, k_{et} decays rapidly, but when $R_{N1-H16} > 6.0$ Å, k_{et} decreases gently. Among the three coupling modes via which the ET reaction occurs, the ET reaction with the largest k_{et} rate is that via coupling mode 3. The values of k_{et} via coupling modes 1 and 2 are almost equal. Overall, the ET occurs chiefly over a range of encounter distance where 2.0 Å $< R_{a-b} <$ 6 .0 Å, and the most favorable coupling mode to the ET is coupling mode 3 in the contact distance range from 2.0 Å to 3.0 Å.

The above analysis indicates that it is not always correct that the ET must experience the most stable coupling mode mechanism. This is to say, like the $C_4H_5N/C_4H_5N^+$ system, that for many systems the most stable coupling structure cannot provide a most favorable geometry for the ET, but perhaps there are many other coupling modes with slightly high energies that are very favorable to the ET. The preliminary investigations on the ET reactivity of some biological molecular systems have indicated this prediction to be reasonable, but it still needs further exploration.

It should be noted that the above analysis is limited to the ET rate and the ET reactivity in the ET step (eq 3), no overall observed ET rate is considered. This is because that for this kind of system, there generally is a stable precursor complex for ET reaction, unlike the transition metal coordination ion pair which has an unstable encounter complex due to the strong repulsion interaction between the donor and the acceptor. Obviously the positive stabilization energy of the stable encounter complex may yield positive contribution to the overall observed ET rate by preequilibrium constant and favors to the ET reaction. However, in general, if the precursor complex is stable, the successor complex also should be stable. So after the ET step finishes, the dissociation of the successor complex must play an important role for the overall observed ET rate. Obviously, the dissociation of the successor complex needs extra energy and may yield negative contribution to overall ET process. The stronger the coupling interaction between the donor and the acceptor, the more stable the encounter complex, and further the more negative the contribution from the dissociation of the successor complex to the overall ET. In particular, for the stronger coupling systems, the stronger coupling interaction has greatly reduced the activation energy, resulting in the ET step being very fast, and meanwhile, this stronger coupling interaction has also increased the stabilization energy of the precursor complex and the dissociation energy of the successor complex, resulting in the dissociation step of the successor complex being very slow. Therefore, for this situation the dissociation step becomes as the dominant one, the rate-limiting step, and the ET step becomes the secondary one in the overall ET reaction process. Obviously, this kind of the ET processes with stronger coupling mode are more complicated, even if the solvent effect is not included. This work aims only at the ET rate problem and focuses on the analysis of the contact distance dependence of the relevant ET kinetics parameters and on the ET reactivity only about the ET step, the overall behaviors will be further investigated.

6. Conclusion

The structural properties and the ET reactivity of pyrrole/pyrrole cation ($C_4H_5N/C_4H_5N^+$) coupling system have been investigated using DFT and MP2 methods with different basis sets in this paper, the main conclusions can be drawn as follows.

(1) The optimizations indicate that there are three different stable coupling complexes for this cationic pair: one face−face coupling complex (complex 1), one side−side coupling complex (complex 2), and one H-bond complex (complex 3). The stability order with the correction for BSSE of the three complexes is complex 1 > complex 2 > complex 3. On the basis of the three stable encounter complexes, three coupling modes have been designed to further explore the contact distance dependence of the ET reactivity of this system; they are referred to coupling modes 1, 2, and 3.

(2) The applicability of DFT methods has been discussed in predicting the dissociation energy curves of the coupling system, especially for those with large contact distance. Results indicate that all DFT methods exhibit the abnormal dissociation behavior, viz., they present an "inverse symmetry breaking" problem, while the Møller−Plesset theory method can reproduce the normal dissociation curves for this kind of systems and then is suitable for further discussion of the contact distance dependence of the kinetics parameters (the activation energy, the coupling matrix element, and the ET rate) of ET reaction. Although DFT methods cannot give reasonable dissociation behavior for the coupling system far from equilibrium, they can yield very accurate results for structural properties and ET reactivity of the coupling system at equilibrium state.

(3) In general, ET can occur over a range of encounter distance. The contact distance dependence of the activation energy, the coupling matrix element, and the ET rate has also been discussed. As to the contact distance dependence of the activation energy, with the contact distance increasing from

about 2.0 to 13.0 Å, the activation energy via three coupling modes deceases first, but after passing a minimum activation energy barrier, it increases. As to the contact distance dependence of the coupling matrix element and the rate of ET via the three coupling modes, they exhibit similar variety tendencies. With the contact distance increasing from about 2.0 to 13.0 Å, both the coupling matrix element and the rate of ET increase at first, after surrounding a maximum, then gradually decrease. ET occurs chiefly over a range of encounter distance where 2.0 Å $< R_{N1-H16} <$ 6.0 Å. For the ET step, the most favorable coupling mode to ET is mode 3 (the H-bond coupling mode) in the contact distance range from 2.0 Å to 3.0 Å. The maximum value of the ET rate is about 5.27×10^9 s^{-1}, it is via coupling mode 3, and the corresponding contact distance, R_{N1-H16}, is about 2.5 Å.

(4) Results have indicated that it is not always true that ET must undergo the most stable coupling mode mechanism. Like this system, the $C_4H_5N/C_4H_5N^+$ system, the most stable coupling structure is coupling mode 1, but the most favorable mode to ET is coupling mode 3. This observation has shown a phenomenon that perhaps the most stable coupling mode cannot provide the most favorable geometry to the ET, but there are other coupling modes with slightly high energy that are very favorable to the ET. The preliminary investigations on the ET reactivity of some biological molecular systems have indicated this prediction to be reasonable, but it still needs further exploration.

(5) It should be noted that the ET reactivity of this kind of coupling system is very complicated, the overall analysis about it is more difficult, not only because there is a complicated solvent effect on the ET process, but also because the ET behavior at different contact distances and coupling orientations may significantly change along with the changes of the contact distance and the coupling orientation. In particular, for the stronger coupling systems, the ET step and the dissociation step of the successor complex may alternatively vary and become as the dominant step along with the change of the contact distance or the coupling orientation. Therefore, the overall behavior including the solvent effect of the ET reactivity of this kind of system needs further investigation.

Acknowledgment. This work is supported by the Foundation for University Key Teacher by the Ministry of Education. The support from the National Natural Science Foundation of China (29973022, 20273040) is also acknowledged.

Supporting Information Available: The vibrational frequencies of monomers and complexes and electron-transfer kinetics parameters for three different coupling modes. This material is available free of charge via the Internet at http://pubs.acs.org.

References and Notes

(1) Herzberg, G.; Huber, K. P. *Molecular Spectra and Molecular Structure.* 4. *Constants of Diatomic Molecules*; Van Nostrand: New York, 1979.
(2) Nelson, R. D.; Lide, D. R.; Maryott, A. A. *Selected Values of Electronic Dipole Moments for Molecules in Gas Phase*; NSRDS No. 10; National Bureau of Standards: Washington, DC, 1967.
(3) Lee, S. Y.; Boo, B. H. *J. Phys. Chem.* **1996**, *100*, 15074.
(4) Jiang, J. C.; Tsai, M. H. *J. Phys. Chem.* A **1997**, *101*, 1982.
(5) Von Niessen, W.; Cederbaum, L. S.; Diercksen, G. H. F. *J. Am. Chem. Soc.* **1976**, *98*, 2066.
(6) Cave, R. J.; Newton, M. D.; Kumar K.; Zimmt, M. B. *J. Phys. Chem.* **1995**, *99*, 17501.
(7) Cave, R. J.; Newton, M. D. *Chem. Phys. Lett.* **1996**, *249*, 15.
(8) Cave, R. J.; Newton, M. D. *J. Chem. Phys.* **1997**, *106*, 9213.
(9) Newton, M. D. *J. Electroanal. Chem.* **1997**, *438*, 3.
(10) Jones, M.; Kurnikov, L. V.; Beratan, D. N. *J. Chem. Phys. A* **2002**, *106*, 2002.
(11) Delahay, P. *Chem. Phys. Lett.* **1982**, *87*, 607.
(12) Delahay, P.; Dziedzic, A. *J. Chem. Phys.* **1984**, *80*, 5793.
(13) Tunuli, M. S.; Khan, S. U. M. *J. Phys. Chem.* **1987**, *91*, 3474.
(14) Lukas, A. S.; Miller S. E.; Wasielewski, M. R. *J. Phys. Chem. B* **2000**, *104*, 931.
(15) Bally, T.; Sastry, G. N. *J. Phys. Chem. A* **1997**, *101*, 7923.
(16) Bu, Y.; Deng, C. *J. Phys. Chem.* **1996**, *100*, 18093.
(17) Bu, Y.; Song, X.; Deng, C. *J. Phys. Chem.* **1999**, *103*, 4485.
(18) Bu, Y.; Cao, Z.; Song, X. *Int. J. Quantum Chem.* **1996**, *57*, 95.
(19) Bu, Y.; Ding, Y.; Deng, C. *J. Mol. Struct.* **1997**, *417*, 69.
(20) Bu, Y.; Deng, C. *J. Phys. Chem.* **1997**, *101*, 1198.
(21) Frisch, M. J.; Trucks, G. W.; Schlegel, H. B.; Gill, P. M. W.; Johnson, B. G.; Robb, M. A.; Cheeseman, J. R.; Keith, T.; Petersson, G. A.; Montgomery, J. A.; Raghavachari, K.; Al-Laham, M. A.; Zakrzewski, V. G.; Ortiz, J. V.; Foresman, J. B.; Peng, C. Y.; Ayala, P. Y.; Chen, W.; Wong, M. W.; Andres, J. L.; Replogle, E. S.; Gomperts, R.; Martin, R. L.; Fox, D. J.; Binkley, J. S.; Defrees, D. J.; Baker, J.; Stewart, J. P.; Head-Gordon, M.; Gonzalez, C.; Pople, J. A. *Gaussian 94*, rev. B.2; Gaussian, Inc.: Pittsburgh, PA, 1995.
(22) Lee, C.; Yang, W.; Parr, R. G. *Phys. Rev.* B **1988**, *37*, 785.
(23) Stephens, P. J.; Devlin, F. J.; Ashvar, C. S.; Chabalowski, C. F.; Frisch, M. J. *Faraday Discuss.* **1994**, *99*, 103.
(24) Perdew, J. P. *Phys. Rev.* B **1986**, *33*, 8822.
(25) Perdew, J. P. *Phys. Rev.* B **1986**, *34*, 7406.
(26) Perdew, J. P.; Wang, Y. *Phys. Rev.* B **1992**, *45*, 13244.
(27) Boys, S. F.; Bernardi, F. *Mol. Phys.* **1970**, *19*, 553.
(28) Xie, Y.; Schaefer, H. F., III; Fu, X. Y.; Liu, R. Z. *J. Phys. Chem.* **1999**, *111*, 2532.
(29) Hrouda, V.; Roeselova, M.; Bally, T. *J. Phys. Chem. A* **1997**, *101*, 3925.
(30) Bu, Y. *J. Phys. Chem.* **1994**, *98*, 2290.
(31) Bu, Y. *J. Phys. Chem.* **1995**, *99*, 11650.
(32) Brunschwig, B. S.; Sutin, N. *Coord. Chem. Rev.* **1999**, *187*, 233.